hydrology

MDPI

Article

Mixed Recharge and Epikarst Role in a Complex Metamorphic Karst Aquifer: The Pollaccia System, Apuan Alps (Tuscany, Italy)

Alessia Nannoni [1,2] and Leonardo Piccini [1,2,*]

[1] Department of Earth Science, Università di Firenze, 50120 Firenze, Italy; alessia.nannoni@unifi.it
[2] Commissione Scientifica—Federazione Speleologica Toscana, 57120 Livorno, Italy
* Correspondence: leonardo.piccini@unifi.it

Abstract: The Apuan Alps (Italy) are an internationally renowned karst region where several karst springs have a mean discharge exceeding 100 L/s, thus representing important water resources. One of the major springs, the Pollaccia, was monitored for approximately one year. This spring drains a structurally complex metamorphic karst aquifer that is characterized by multiple hydrologic sectors with variable recharge and infiltration styles. Spring discharge, water temperature, and electrical conductivity were compared to precipitation data, and time lag analysis was performed on 27 storm hydro/thermo/chemographs (HTC-graphs) that occurred in different hydrological phases. A marked seasonality was observed for all the monitored parameters and for the measured lags. The comparison of the storm HTC-graphs with no precipitation phases permitted recognition of the differential contribution of the various sectors. The Pollaccia's hydrodynamic behavior was related to three different scenarios in the recharge area: (1) allogenic runoff recharge in the noncarbonate sectors; (2) autogenic recharge and runoff over the steeply dipping marble outcrops, characterized by fast epiphreatic flow through master conduits and low epikarst storage; (3) autogenic recharge through highly fractured, gently dipping marble outcrops, characterized by quick hydraulic pressure transfer to the phreatic zone and relevant epikarst storage.

Keywords: karst system; hydrological monitoring; structural setting; metamorphic aquifer; Apuan Alps

Citation: Nannoni, A.; Piccini, L. Mixed Recharge and Epikarst Role in a Complex Metamorphic Karst Aquifer: The Pollaccia System, Apuan Alps (Tuscany, Italy). *Hydrology* **2022**, *9*, 83. https://doi.org/10.3390/hydrology9050083

Academic Editor: Mahmoud Sherif

Received: 31 March 2022
Accepted: 8 May 2022
Published: 11 May 2022

1. Introduction

The hydrogeological setting of karst aquifers is usually complex due to their heterogeneity in porosity, permeability, groundwater flow dynamic, water storage, and recharge style [1]. Two main types of recharges occur in karst catchments: allogenic and autogenic. The former occurs where surface runoff draining low permeable and poorly soluble terrains infiltrates into an adjacent permeable and highly soluble carbonate bedrock. The latter happens directly on the surface of karstic outcrops, and it can be further subdivided in two types: diffuse (i.e., through soil and fissures) and concentrated (i.e., by sinkholes) [2,3]. Recharge type directly influences water flow in the vadose zone because concentrated infiltration does not pass through the epikarst zone, in contrast to diffuse recharge [4]. The term "epikarst" commonly refers to the topmost part of karst systems that consists of highly weathered carbonate rocks with high secondary porosity [5]. At depth, it gradually passes to the main part of the vadose zone (i.e., the transmission zone), which is made up mostly of unweathered rocks. Part of the water that flows through the epikarst is temporarily stored and slowly released downward into the transmission zone. In other words, the epikarst acts as a shallow, perched aquifer where infiltrating water acquires an increasing dissolved ion content as a function of the residence time. This perched aquifer is responsible for a delayed recharge, and it can sustain vadose percolation during prolonged droughts [6]. Epikarst can be discontinuous and, consequently, its hydrologic role can be reduced or irrelevant. There are also cases where it has not developed, or it was completely removed by geomorphic processes such as glacial or runoff erosion [5]. Epikarst's storage capacity

is primary related to its maturity and to the permeability contrast occurring between its bottom part and the underlying transmission zone. In the phreatic/saturated zone, water flow can occur either in a diffuse manner through interconnected fissures or through high hydraulic–conductivity conduits. The position, geometry, and interaction of the conduits with the rock matrix and fissures, which are commonly responsible for most of the water storage, are largely unknown [7–9]. Therefore, different water storage components can contribute to groundwater flow, and it is often difficult to recognize each of them.

Karst spring hydrographs represent the output signal of the interaction between the recharge waters and the water already stored in different aquifer sectors. Conduit-dominated karst systems are characterized by rapid and large variations in physical and chemical parameters, in response to precipitation or snowmelt, as opposed to dispersive circulation systems [10]. The former systems are composed of an organized drainage network of major conduits (i.e., highly permeable) and secondary drains that quickly discharge the incoming neo-infiltrating water and where water predominantly moves as free surface flow. The phreatic zone is absent or limited in these systems (though full pipe sections can occur in the lower part of the aquifer). The simultaneous decreases in water temperature and electrical conductivity during a discharge peak is their typical hydrodynamic response because the neo-infiltrating water quickly replaces the water circulating in the system (prevalent substitution/dilution). Eventually, short-lasting increases in water temperature and electrical conductivity occur at the flood's beginning due to the remobilization of the water stored in the final phreatic sectors (i.e., piston flow phenomenon).

Continuous monitoring of spring discharge (Q), water temperature (T_w), and specific electrical conductivity (EC_{sp}) is the main method for studying the hydrodynamics of karst springs (e.g., [7,11,12]). The comparison of the spring hydrograph (Q), thermograph (T_w), and chemograph (EC_{sp}) permits investigation of the aquifer architecture and its functioning across the hydrologic year or at the single-storm scale (e.g., [10,13–15]). From this perspective, the lag analysis between the precipitation impulse, Q, T_w, and EC_{sp} variations can be particularly useful, although few works deal with the detailed $Q/T_w/EC_{sp}$ analysis at the single-storm scale [16–18]. Water temperature and electrical conductivity are nonconservative tracers that provide insight into surface/groundwater interactions, groundwater–rock heat exchanges, mixing processes, and recharge modes [19–21].

Drought phases analysis and forecast have become widely used approaches in karst hydrology, because droughts pose critical problems in water management. Moreover, the risk of severe dry conditions is becoming progressively higher due to climate change, and karst aquifers are particularly vulnerable under changing climate conditions [22,23]. However, most of the work on this topic is based on the comparison of seasonal and/or long-term spring discharge data and rainfall patterns [24–27]. The comparison of karst spring hydrographs, thermographs, and chemographs during drought phases has not been investigated in detail to infer hydrologic sectors that contribute to spring flow.

Generally, marble karst aquifers are characterized by lower primary and secondary porosities and permeability than the non-metamorphosed aquifers [28–30]. Groundwater drainage in metamorphic carbonates shows peculiar structures with reduced infiltration and storage with respect to non-metamorphosed carbonate massifs. Moreover, morphological processes and regional tectonics are commonly responsible for the fragmentation and/or juxtaposition of hydro-structures with contrasting characteristics, shaping complex catchments with sectors having different recharge styles and different hydrodynamic behaviors [31–34].

In recent years, the Federazione Speleologica Toscana (Tuscan Speleological Federation), in collaboration with the Department of Earth Science (Università degli Studi di Firenze), carried out a study of major karst systems in the Apuan Alps, in northwestern Tuscany (Italy), through the physical–chemical monitoring of springs and dye tests. Due to its geological structure and the high degree of hydrogeological knowledge, this karst region is a key area worldwide for the study of the hydrology of metamorphic karst aquifers. This paper presents the results of the monitoring of one of the major Apuan karst springs, named

Pollaccia, to unravel the complex functioning of a metamorphic karst aquifer strongly controlled by the local structural setting. Catchment complexity determines variable recharge styles and infiltration rates, as well as the occurrence of different hydrological sectors with contrasting hydrodynamic behaviors during subsequent hydrologic phases. The approach proposed in this investigation was based on three methods: (1) hydrograph, thermograph, and chemograph analyses at the single-storm and (2) at the seasonal scale; (3) analysis of the precipitation pattern's influence on the spring hydrodynamics. Furthermore, the monitored period offered an opportunity to carry out this investigation during an anomalous drought phase that permitted emphasizing the role of epikarst storage in specific sectors of the Pollaccia spring catchment.

2. Study Area

2.1. Geomorphological and Geological Setting

The Apuan Alps have a peculiar alpine-like landscape that is the result of its complex structural setting and differential erosion. Weathering and denudation processes have produced a landscape where the highest and steepest reliefs consist mainly of carbonate formations, whereas valleys are often composed of shale. Presently, surface karst dissolution is limited because of the steep relief. On the contrary, a lower relief allowed for the development of extended epikarst landforms and large cave systems in the early Pleistocene [35]. The geological structure greatly influences the geomorphological features of the karst areas. The epikarst is scarce and discontinuous in areas with sub-vertical bedding, steep slopes, and non-pervasive fracturing (Figure 1a). On the contrary, the epikarst is well-developed in areas with sub-horizontal bedding surfaces and more pervasive fracturing. The latter areas are characterized by karren fields, grikes, and very deep fissures (Figure 1b). This different morphology strongly influences the infiltration mode, which is reduced in the first case, being concentrated in absorption points localized along the streams, and high and diffuse in the second case. This arrangement can be observed in the Pollaccia catchment: most of the marble outcrops show a poorly developed epikarst, steeply dipping bedding, and relatively moderate fracturing. The Pania della Croce mountain group is the only exception (hereafter referred to as "Panie"; Figure 2): the epikarst is clearly present, and multiple sets of vertical fractures with variable strikes and apertures crosscut the sub-horizontal marble sequence.

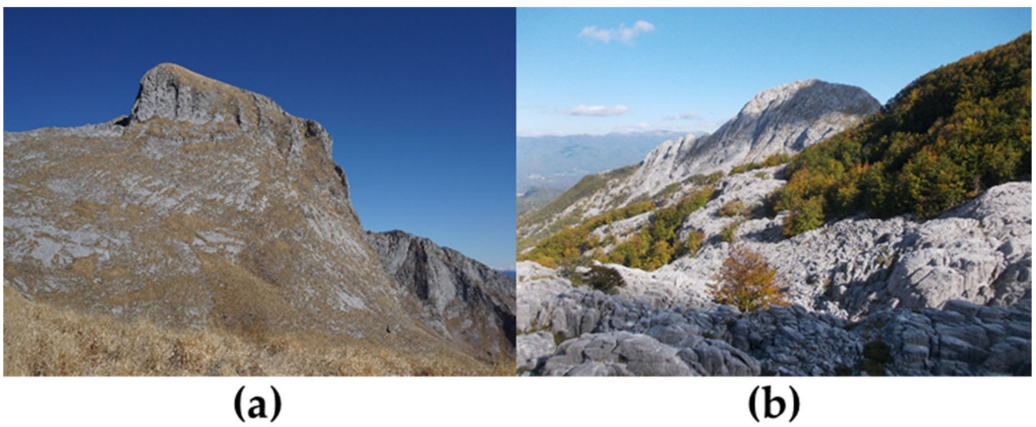

Figure 1. (**a**) Marble outcrops with a low development of epikarst and a low infiltration rate (M. Sumbra); (**b**) Marble outcrops with a well-developed epikarst and a high infiltration rate (Panie group). Both areas belong to the catchment area of the Pollaccia spring.

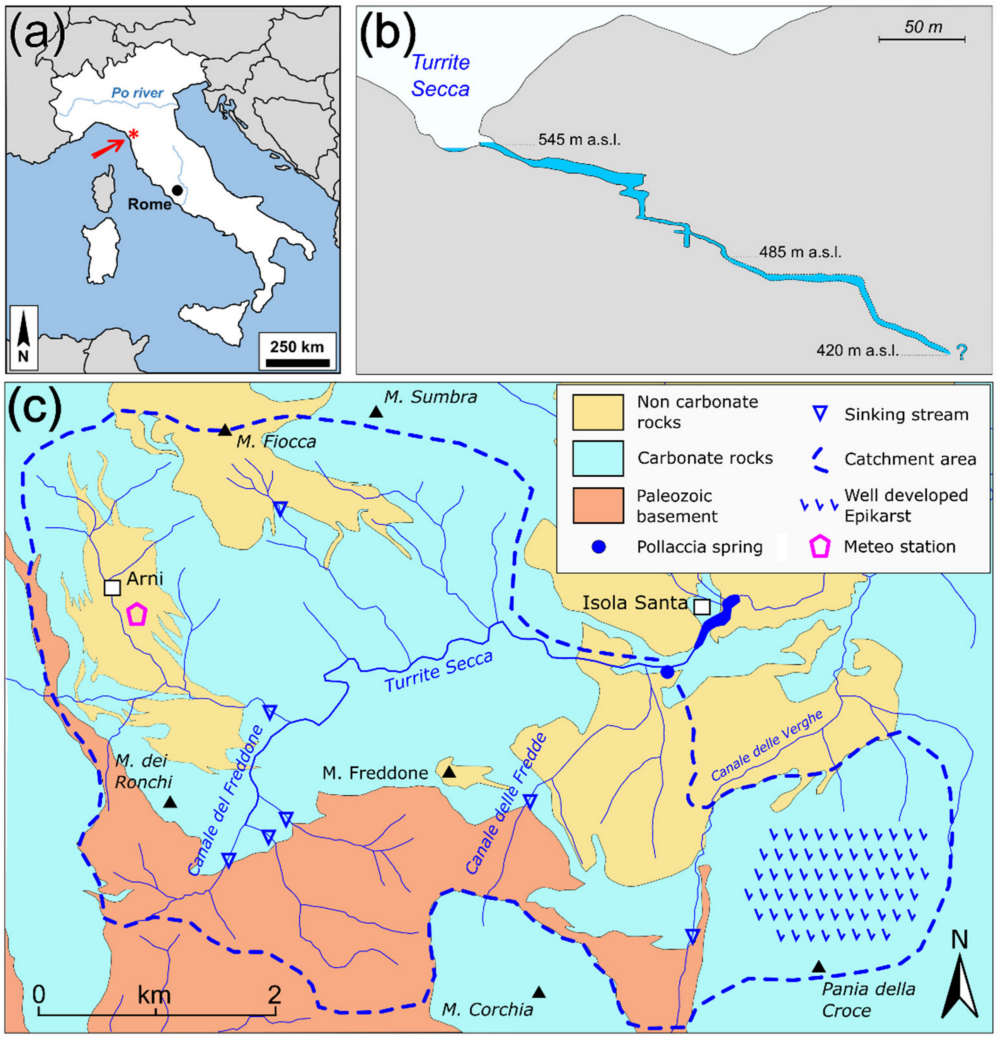

Figure 2. (**a**) Location map; the red arrow indicates the study area; (**b**) cross-section of the deep phreatic tube explored by divers down to −120 m; (**c**) hydrogeological map of the catchment area feeding the Pollaccia spring.

The geological setting of the Apuan Alps is very complex due to the occurrence of several overlapped tectonic units. The lowermost units (i.e., Apuane and Massa) are characterized by a green-schist facies metamorphism [36]; both units were overthrusted by non-metamorphic units and were exhumed during a Late Miocene to Pliocene extensive tectonic phase [37]. The Apuane Unit consists of a meta-sedimentary sequence deposited on a metamorphic Paleozoic basement made up by phyllites and metavolcanics. The sedimentary sequence was formed upward by polygenic conglomerates (Lower to Middle Triassic), dolostone and limestone of carbonate platform (Carnic–Sinemurian), calcareous to siliceous pelagic rocks (Pliensbachian–Lower Oligocene), and turbidites (Upper Oligocene) [38]. Large-scale NE verging isoclinal folds characterize the structural setting of the metamorphic complex. Two main folding phases were recognized: the first one was syn-metamorphic (27–20 Ma), followed by a secondary one (11–8 Ma) [37]. A late extensional tectonic phase caused the uplift of the massif along NW–SE and NE–SW striking faults. The exposed metamorphic complex is not significantly affected by large post-orogeny faulting, but a uniformly oriented system of minor faults and joints was recognized [39].

The study area comprised metamorphic terrains that belong either to the noncarbonate Paleozoic basement (Arni-M. Fiocca sector), to the Triassic–Jurassic carbonate sequence, and to the noncarbonate sediments (M. dei Ronchi and Corchia N side/Canale delle Fredde sectors).

2.2. Hydrogeology

The Pollaccia is one of the most investigated springs of the Apuan Alps ([34,40] and references therein). It has the second discharge among the Apuan springs, and the largest of the Serchio River basin. The water discharges along the Turrite Secca valley at 540 m asl and flows up from an ascending submerged conduit (valclusian-type spring) which was explored by cave divers down to a 120 m depth and for a total length exceeding 500 m (Figure 2b). Piccini [40] provides an average discharge of 0.8 m^3/s. Several dye tracer tests were performed with charcoal detectors or with a fluorimeter to define the catchment of the Pollaccia spring. Mean flow velocities extrapolated with these tests were 14.4 m/h in the SW part of the catchment (M. dei Ronchi, Figure 2), 8.7 to 20.8 m/h in the SE area (Pania della Croce), and 88 m/h in the southern sector (N side of M. Corchia, Figure 2a) [41].

3. Methods

The Pollaccia spring was monitored for 384 days (from 6 November 2011 to 23 November 2012), although some interruptions occurred during the driest periods, by means of a multiparametric probe (model Eijke–kamp—CTD DIVER), measuring water pressure, temperature (T_w), electrical conductivity (EC), and a barometric probe (model Eijke–kamp—CTD BARO) measuring atmospheric pressure and air temperature. The pressure resolution of both probes was 2 mm_{water} with an accuracy of 5 mm_{water}. The two pressure sensors measured the water load on the immersed probe and the atmospheric pressure, respectively. The difference between the pressure measured by the diver and the atmospheric pressure provided the height of the water level above the immersed probe. A 30 cm thick rectangular weir occurs 7 m downstream of the spring. Discharge was calculated by measuring the height of water level above the overflow threshold and applying the conventional simplified formula for a broad-crested rectangular weir [42]:

$$Q = 0.4 \cdot h \cdot L \cdot \sqrt{(2 \cdot g \cdot h)} \quad (1)$$

where 0.4 is a nondimensional, experimental constant (efflux coefficient) that is related to the weir geometry, **h** is the water height above the rim of the weir, **L** is the weir width (5.37 m), and **g** the gravity acceleration. The discharge values obtained with this equation did not account for approximately 20–50 L/s of water flowing from minor outlets just downstream of the main outlet.

The water temperature sensor had a resolution of 0.01 °C and an accuracy of ±0.5 °C. The electrical conductivity was measured with a resolution of 0.1% and a reading accuracy of 1% (approximately 2–3 µS/cm). Conductivity data were converted to specific conductivity at the reference temperature of 25 °C (EC_{sp}) with the following equation:

$$EC_{sp} = 100/[100 + \theta(T_w - 25)] \cdot EC \quad (2)$$

where **EC** is the electrical conductivity at the sample temperature $\mathbf{T_w}$, and θ is a temperature coefficient equal to 1.91%/°C that was provided by the manufacturer (Van Essen Instruments). A sampling time of 30 min was set for all the probes. During the summer seasons, there were some periods without measurements when the water level decreased below the probe position because of low-flow conditions. For these periods, the water level was extrapolated according to the inferred exhaustion curve.

Precipitation data were collected by the Campagrina meteorological station (807 m asl, western Turrite Secca basin, Figure 2c) of the Regional Hydrological Service of Tuscany (SIR database; station code: TOS02000241; https://www.sir.toscana.it/consistenza-rete, accessed 1 December 2020). This station can be considered as representative of the precipitation regime in the catchment area. The sampling frequency was 15 min for precipitation, but the data were aggregated at 30 min intervals for comparison with the Pollaccia hydrological data.

Storm Hydrographs and Lags Measurements

A total of 27 storm events were analyzed during four hydrological phases: autumn and spring recharges, winter and summer droughts. The hydrological phases were defined according to the effect that the infiltration exerted on the water baseflow during the monitored hydrological year. Precipitation during the autumn and spring seasons caused high infiltration rates and, consequently, the baseflow tended to increase during both seasons (autumn and spring recharge = AR and SR). Scarce to absent precipitation caused a winter and a summer drought phase (WDr and SDr). During the monitoring period, two types of storm hydrographs could be distinguished: simple and complex (i.e., multiple) ones. The former consisted of well-defined single discharge peaks (Figure 3a), whereas the latter were composed of consecutive peaks because of multiple precipitation events (Figure 3b). The parameters considered in this study are listed in Table 1 (e.g., [43]).

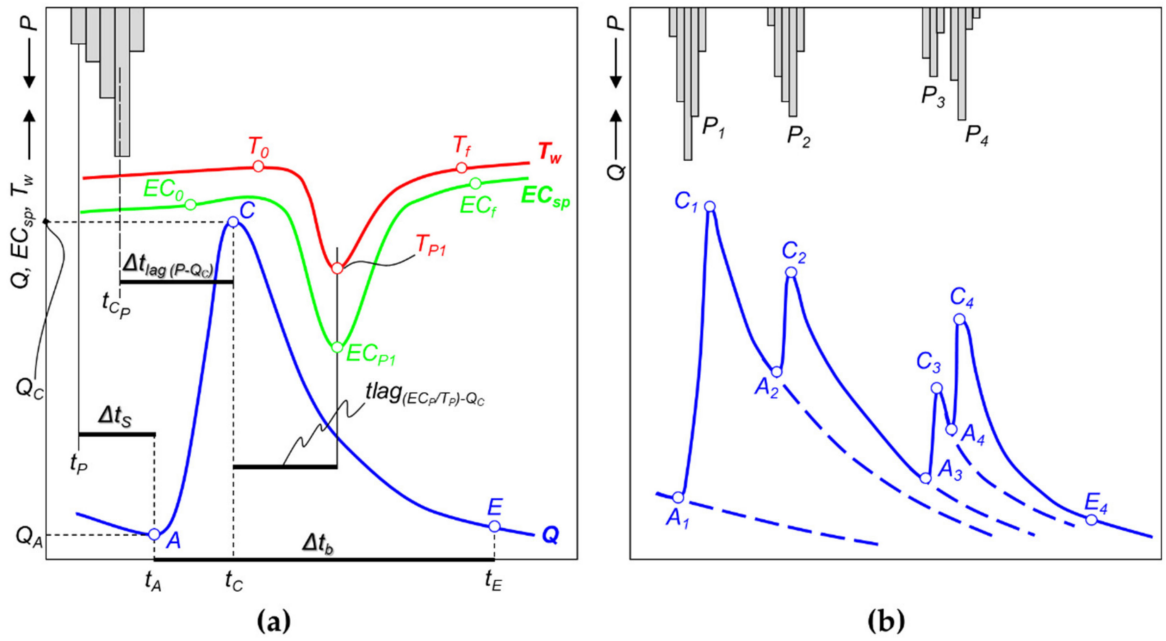

Figure 3. (**a**) Simple storm HTC-graph and its components: hydrograph (Q), thermograph (T_w), and chemograph (EC_{sp}); (**b**) complex storm hydrograph. Redrawn after [43].

Table 1. Storm hydrograph, thermograph, and chemograph parameters considered in this study. The most important parameters are described in Figure 3, whereas the complete list with the values for each of them is provided in the Supplementary Material (SM).

Parameter	Definition
Rising limb (A-C/concentration time (Δt_C) (h)	Storm hydrograph segment between the beginning of the flow increase (Q_A) and the the maximum discharge (Q_C)
Q_C-Q_A (m^3/s)	Magnitude of the discharge increase
Falling limb (C-E)/falling time (Δt_f)	Storm hydrograph segment between the maximum discharge (Q_C) and the end of the storm hydrograph (Q_E).
Storm hydrograph duration (Δt_b)	Time elapsed between the beginning (A) and the end (E) of the storm hydrograph
Δt_P (h)	Time interval with no significant precipitation antecedent for each storm event
t_P	Timing of the onset of precipitation
Starting time (Δts) (h)	Time elapsed between the onset of precipitation (t_P) and the beginning of the rising limb (t_A)

Table 1. *Cont.*

Parameter	Definition
t_{CP}	Timing of the centroid of precipitation
P_{max} (mm/30 min)	Maximum precipitation intensity
P_{tot} (mm)	Total precipitation of a storm event
P_{rate} (mm/h)	Precipitation rate
Lag time ($\Delta t\ lag_{(P-Qc)}$)	Time elapsed between the centroid of the precipitation pulse (t_P) and the maximum discharge (Q_C)
T_0/EC_0	Temperature/specific conductivity value at the beginning of the oscillations caused by the storm event
T_1/EC_1	Temperature/specific conductivity value of the first (positive or negative) peak caused by the storm event
T_f/EC_f	Temperature/specific conductivity value at the end of the storm event
$\Delta T_{P1-0}/\Delta EC_{P1-0}$	Temperature/specific conductivity variation between T_1/EC_1 and T_0/EC_0
$\Delta T_{f-0}/\Delta EC_{f-0}$	Temperature/specific conductivity variation between T_f/EC_f and T_0/EC_0
$tlag_{(T/EC)-Qc}$	Time elapsed between the maximum discharge (Q_C) and T_{P1}/EC_{P1}

The complex storm hydrographs were analyzed with the same method as the simple storms, although the information they provided was more difficult to unravel. The parameters were measured for each individual peak, while the falling time was measured only for the last significative peak. The parameters of each meteorological event and the thermograph and chemograph corresponding to each storm hydrograph were also considered, calculating the lag time between the Q and T/EC peaks (Figure 3a). The correlation coefficients were calculated for the precipitation data and for the storm hydrographs' parameters by means of Pearson correlation analysis to compare the precipitation variability with the hydrological behaviors. P_{tot}, P_{rate}, and P_{max} were taken as indicative of the storm event's magnitude, whereas Q_C–Q_A for the flood's magnitude. The Δt_S, Δt_C, and $\Delta t\ lag_{(P-Qc)}$ provided insight into the spring's response to the precipitation, and Δt_P was a measure of the wet/dry conditions antecedent to each storm event. This analysis was performed on a total of 37 discharge peaks from the 27 storm hydrographs including the multiple ones.

4. Results

4.1. Hydrological Monitoring

Figure 4 shows the HTC-graph (Hydrograph—Q, Thermograph—T_w, and Chemograph—EC_{sp}) for the Pollaccia spring compared to the precipitation data measured at the Campagrina meteorological station. The data were reported with a 30 min time step. The statistics regarding the hydrological and meteorological monitoring are shown in Table 2. Different hydrological phases were recognized throughout the whole HTC-graph: two autumn recharge phases (AR: November 2011 and October to November 2012); a winter drought phase (WDr: from the end of November 2011 to the end of March 2012); a spring recharge phase (SR: April to May 2012); a summer drought phase (SDr: June to September 2012).

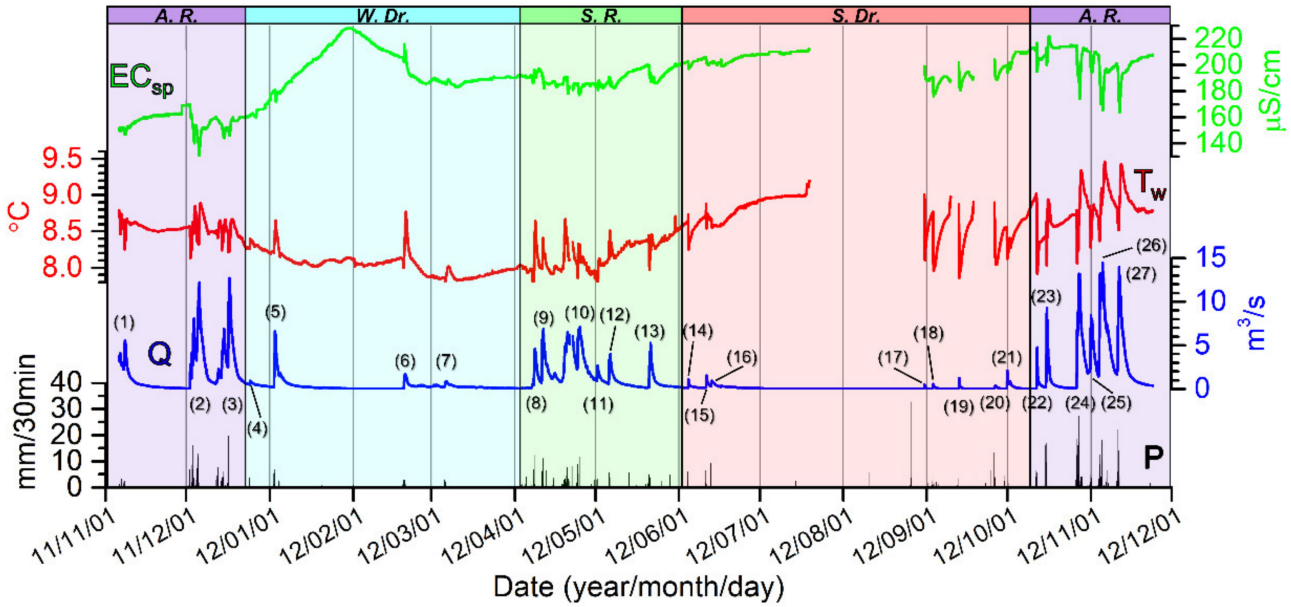

Figure 4. HTC-graph (Q–T_w–EC_{sp}) of the Pollaccia spring. Precipitation data (P) were taken at the Campagrina meteorological station. The colors highlight the different hydrological phases: purple, cyan, green, and red represent the autumn recharge (A.R.), the winter drought (W.Dr.), the spring recharge (S.R.), and the summer drought (S.Dr.) phases, respectively. The numbers in brackets refer to the storm hydrographs analyzed for this study.

Discharge varied between 0.025 and 14.5 m^3/s. Given the hidden sources downstream of the main outflow, the maximum discharge probably reached 15 m^3/s for the monitored period, whereas the average discharge was equal to 0.92 m^3/s. The spring response to storm events was rather fast, with lag times of a few hours (Table 2). The highest discharge values were observed during the two autumn seasons (November 2011 and 2012), whereas the peak discharge values were lower during the spring season (from April to the end of May 2012). This marked difference in discharge could be related to the precipitation pattern. In fact, the total amount of precipitation that occurred in the September to December 2011, February to May 2012, and September to December 2012 time intervals were 1539, 933, and 1946 mm, respectively (Figure 5). Moreover, the 2012 spring season was preceded by a low precipitation phase (total P from 2011/12 to 2012/02 = 877 mm, but over 75% of the precipitation was concentrated in the first half of December 2011), whereas the September to December 2011 and the October to December 2012 intervals were the rainiest periods of 2011 and 2012, respectively (Figure 5). Two drought phases were observed: the first one occurred from the end of December 2011 to the end of March 2012; the second one occurred from mid-June to mid-September 2012. The former drought was briefly disturbed by four small rain events (4, 5, 6, and 7 in Figure 4).

The year 2012 was characterized by an anomalous seasonal variability in precipitations, showing a prolonged winter drought and extremely heavy rainfalls during autumn. Moreover, 75% of the spring precipitation occurred in 23 days during April. This unusual circumstance probably enhanced hydrodynamic phenomena that are not always observable.

Table 2. Summary statistics of the main parameters of the storm HTC-graph analysis. More information on the analyzed storm HTC-graphs can be found in the Supplementary Materials (SM).

Parameter	Statistical Index	Value
Q_c–Q_A	Minimum	0.28
	Maximum	13.15
	Mean	3.96
	Median	2.78
P_{rate} (mm/h)	Minimum	0.00
	Maximum	30.84
	Mean	6.48
	Median	4.84
Δt_P (h)	Minimum	1.50
	Maximum	577.00
	Mean	105.84
	Median	59.00
Δt_S (h)	Minimum	0.00
	Maximum	8.00
	Mean	3.18
	Median	2.50
$\Delta t\ lag_{(P-Qc)}$ (h)	Minimum	2.00
	Maximum	14.00
	Mean	5.65
	Median	5.00
$\Delta t\ lag_{(Tpeak1-Qc)}$ (h)	Minimum	−14.00
	Maximum	4.50
	Mean	−2.35
	Median	−2.00
$\Delta t\ lag_{(ECpeak1-Qc)}$ (h)	Minimum	−6.50
	Maximum	10.50
	Mean	1.62
	Median	1.50

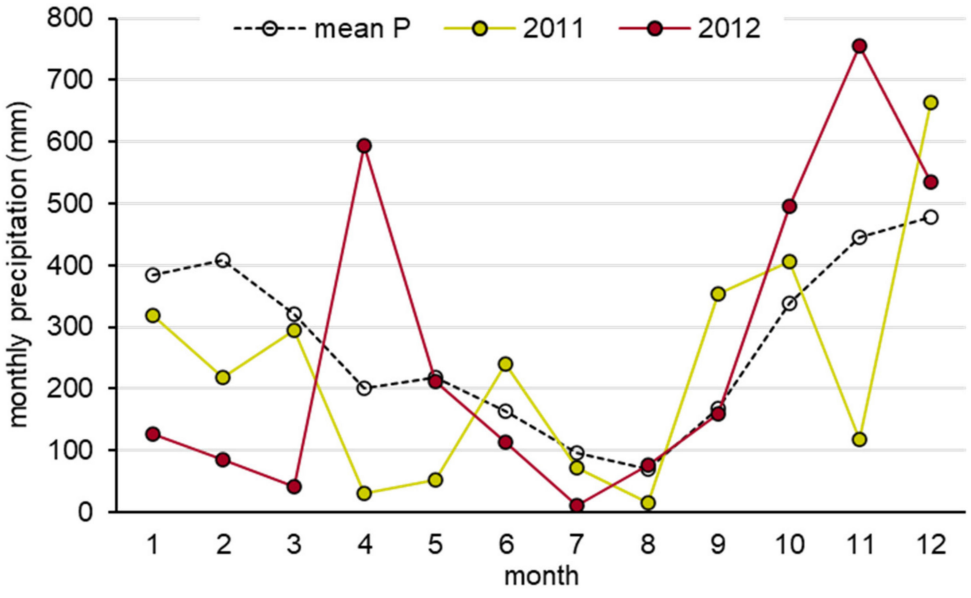

Figure 5. Comparison between the mean monthly precipitation (2010–2020) and the monthly values for the 2011 and 2012 years. Data were collected by the Campagrina meteorological station (station code: TOS02000241; https://www.sir.toscana.it/consistenza-rete, accessed on 1 December 2020).

Water temperature showed marked seasonal trends: the lowest mean values were observed during the winter and spring phases, whereas the highest ones were recorded during the summer drought (end of July 2012) and autumn recharge (November 2012, Figures 4 and 6a). The temperature ranged between 7.8 and 9.5 °C with a mean value of 8.4 °C. The minimum values (measured on 7 April and the 1 May 2012) were due to the cold meltwater. The highest absolute T_w values were measured in November 2012, but the highest mean values were recorded during the summer drought phase. T_w settled to approximately 8 °C during the winter drought phase. The sharpest T_w oscillations occurred between September and November 2012, although there were some gaps because the sensor was not always fully submerged. The T_w and EC_{sp} seasonal trends showed opposite oscillations during AR and WDr and during in-phase oscillations during SR and SDr (Figure 4). The specific electrical conductivity ranged between 131 and 228 µS/cm with a mean value of 192 µS/cm. The values acquired during autumn recharge phase showed the highest dispersion and the lowest mean value, whereas those recorded during spring discharge and summer drought were more concentrated at approximately 190 and 210 µS/cm, respectively. Winter drought values had a higher variability than the SDr and SR data and a mean value second only to the summer one (Figure 6b).

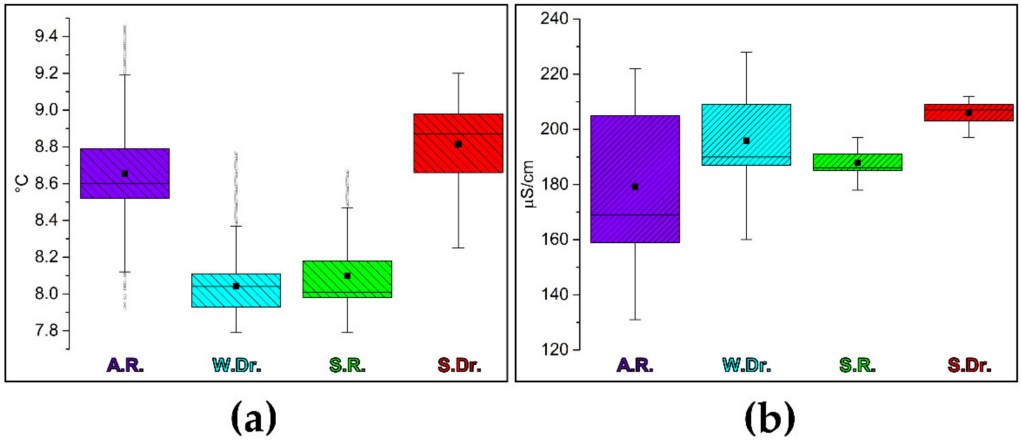

Figure 6. Boxplots of the water temperature (**a**) and the specific electrical conductivity (**b**) data of the Pollaccia spring. Data were grouped according to the different hydrological phases: autumn recharge (A.R.), winter drought (W.Dr.), spring recharge (S.R.), and summer drought (S.Dr.).

A very interesting event was the increase/decrease phase of the EC_{sp} that was observed during the winter drought (from 24 December 2011 to the end of January 2012). During this period, EC_{sp} rose from 150 to 230 µS/cm when discharge was decreasing due to the lack of rain and snow melt. This conductivity fluctuation was accompanied by a slight decrease in water temperature. From the end of January 2012, EC_{sp} started to decrease progressively without evidence of flow variations or meltwater injections that typically occur with daily air temperature fluctuations. EC_{sp} again started to increase constantly from the middle of April to the end of July, although with many small but significant variations (approximately 20 µS/cm) due to the recharge events in spring season.

4.2. Storm HTC-Graph Analysis

The storm HTC-graph analysis was performed on most of the recharge events that occurred during the monitoring period. Some of the events that occurred during the snowmelt caused irregular hydrographs; therefore, they were not analyzed. Table 2 reports the summary statistics of the most relevant measured parameters, whereas the complete list of parameters can be found in the Supplementary Materials (SM).

The Pollaccia spring exhibited short P-Q time lags ($\Delta t\ lag_{(P-Qc)}$) with a mean value of 5.65 h and a range of variation equal to 12 h (Table 2). The lag times did not differ significantly between the simple and complex storm hydrographs; in fact, the minimum,

maximum, and mean/median values did not change significantly including or excluding consecutive Q peaks of complex events (see SM). The application of the Pearson correlation analysis to the whole dataset revealed, as expected, a positive correlation between the discharge increment (Q_C-Q_A) and the magnitude of the storm (P duration, P_{tot}, and P_{max}). No clear correlations were found between the storm magnitude and the P-Q lags or between the storm hydrograph magnitude and the dry interval preceding the storm event (Table 3).

Table 3. Pearson correlation matrix of the precipitation and storm hydrograph parameters. The underlined values are significant at the 0.05 level.

	Q_C–Q_A	P Duration	P_{tot}	P_{rate}	P_{max}	Δt_P	Δt_S	Δt_C	Δt $Lag_{(P-Qc)}$
Q_C–Q_A									
P duration	0.658								
P_{tot}	0.761	0.601							
P_{rate}	0.101	−0.230	0.472						
P_{max}	0.653	0.256	0.695	0.619					
Δt_P	−0.072	0.172	−0.036	−0.099	−0.112				
Δt_S	−0.147	0.341	−0.068	−0.392	−0.383	0.181			
Δt_C	0.615	0.918	0.618	−0.135	0.332	0.156	0.163		
Δt $lag_{(P-Qc)}$	0.147	0.266	0.182	−0.111	−0.029	0.088	0.225	0.382	

However, grouping the events according to the hydrological phase shows that the autumnal and winter storm hydrographs had mean $\Delta t\ lag_{(P-Qc)}$ values and variability ranges higher than those that occurred in spring and summer (Figure 7). The winter drought data show the highest variability, but this could be an artifact due to the small number of events. The summer drought events had the lowest median values; therefore, the quickest responses to precipitation occurred during this hydrologic phase, followed by the storms that occurred during the spring discharge phase.

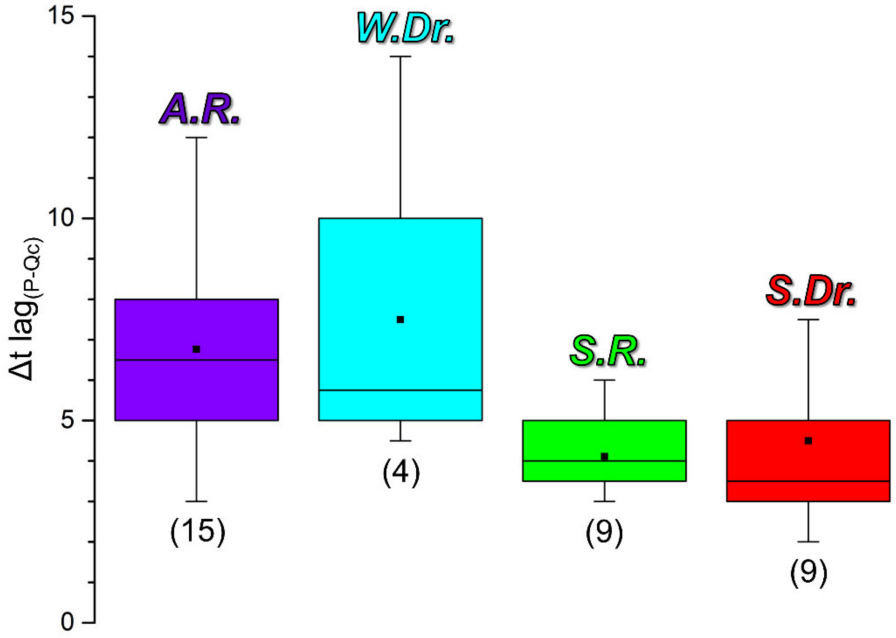

Figure 7. Boxplots of the P-Q lag times ($\Delta t\ lag_{(P-Qc)}$) observed at the Pollaccia spring. Data were grouped according to the hydrological phases: autumn recharge (*A.R.*), winter drought (*W.Dr.*), spring recharge (*S.R.*), and summer drought (*S.Dr.*). The numbers in the brackets refer to the number of storm hydrographs included in each group.

The lag times between the maximum discharge peak and the first temperature peak showed a mean value of −2.35 h, implying that the negative or positive T_w oscillations

occurred during the rising limb of the storm hydrograph or during smaller Q peaks in the case of irregular/multiple storm hydrographs. The longest positive lag between the first T_w peak (T_{P1}) and the Q_c was 4.50 h, whereas the longest negative one was equal to −14.00 h. On average, EC_{P1} had a mean lag with respect to Q_c equal to 1.62 h, whereas the longest positive and negative lags were 10.50 and −6.50 h, respectively.

The three storm HTC-graphs shown in Figure 8 are representative of different responses patterns characterized by single discharge peaks with different magnitudes but similar $\Delta t\ lag_{(P-Qc)}$ (5–6 h; Table 2, SM).

Table 4. Analyzed storm hydrographs. AR = autumn recharge; WDr = winter drought; SR = spring recharge; SDr = summer drought; L/M/H-Q_C = Low/Medium/High peak magnitude ($L-Q_C < 4\ m^3/s$, $4\ m^3/s \leq M-Q_C \leq 8\ m^3/s$, and $H-Q_C > 8\ m^3/s$); + = positive peak/increase; − = negative peak/decrease; d = dilution; p = piston flow (the T/EC fluctuation and the hydrodynamic response in brackets are weaker than the ones without brackets; the labels are time ordered).

Event	Hydrologic Phase	Peak Magnitude	T Fluctuation	EC Fluctuation	Hydrodynamic Response
1	AR	M-Q_C	−	−	d
2	AR	H-Q_C	−	−	d
3	AR	H-Q_C	−	−	d
4	WDr	L-Q_C	+	(+)	(p)
5	WDr	M-Q_C	+, −	(+), −	(p), d
6	WDr	L-Q_C	+	+, +	p, p
7	WDr	L-Q_C	(−), +	(−), +	(d), p
8	SR	M-Q_C	−, +, (−)	−, +, (−)	d, p, (d)
9	SR	M-Q_C	+	−	d
10	SR	M-Q_C	−	−	d
11	SR	L-Q_C	−, (+)	−, (+)	d, (p)
12	SR	L-Q_C	+, −	+, −	p, d
13	SR	L-Q_C	−, +	−, −	d, d
14	SDr	L-Q_C	(+), −	(+), −	(p), d
15	SDr	L-Q_C	(+), −	−	d
16	SDr	L-Q_C	(+)	(+)	(p)
17	SDr	L-Q_C	−	−	d
18	SDr	L-Q_C	−	−	d
19	SDr	L-Q_C	−	−	d
20	SDr	L-Q_C	(+), −	(+), −	(p), d
21	SDr	L-Q_C	−, +	−, +	d, p
22	AR	M-Q_C	−	(+), −	(p), d
23	AR	H-Q_C	(+), −, +	(+), −, +	(p), d, p
24	AR	H Q_C	−, +	−	d
25	AR	H-Q_C	−	−	d
26	AR	H Q_C	−, +	−, −	d, d
27	AR	H-Q_C	−, +	−	d

The first one (Figure 8a) occurred in winter and showed a small discharge increase ($Q_c = 1.69\ m^3/s$). The precipitation event that triggered the hydrodynamic response was characterized by a low P_{rate} (2.57 mm/h). The simultaneous occurrence of a weak meteorological event, the antecedent drought conditions, and eventual snowmelt contribution to recharge was probably the cause of the gentle slope of both the rising and falling limbs (see also $\Delta t_c = 16$ h and $\Delta t_f = 28$ h). The thermograph and the chemograph showed in-phase oscillations, although T_w variations were much broader than those observed for EC_{sp}. First, both slightly decreased probably because of localized infiltration in the proximal areas; then, both parameters' values increased significantly. The recovery time for Q, T_w, and EC_{sp} to return to pre-storm values lasted 3–4 days.

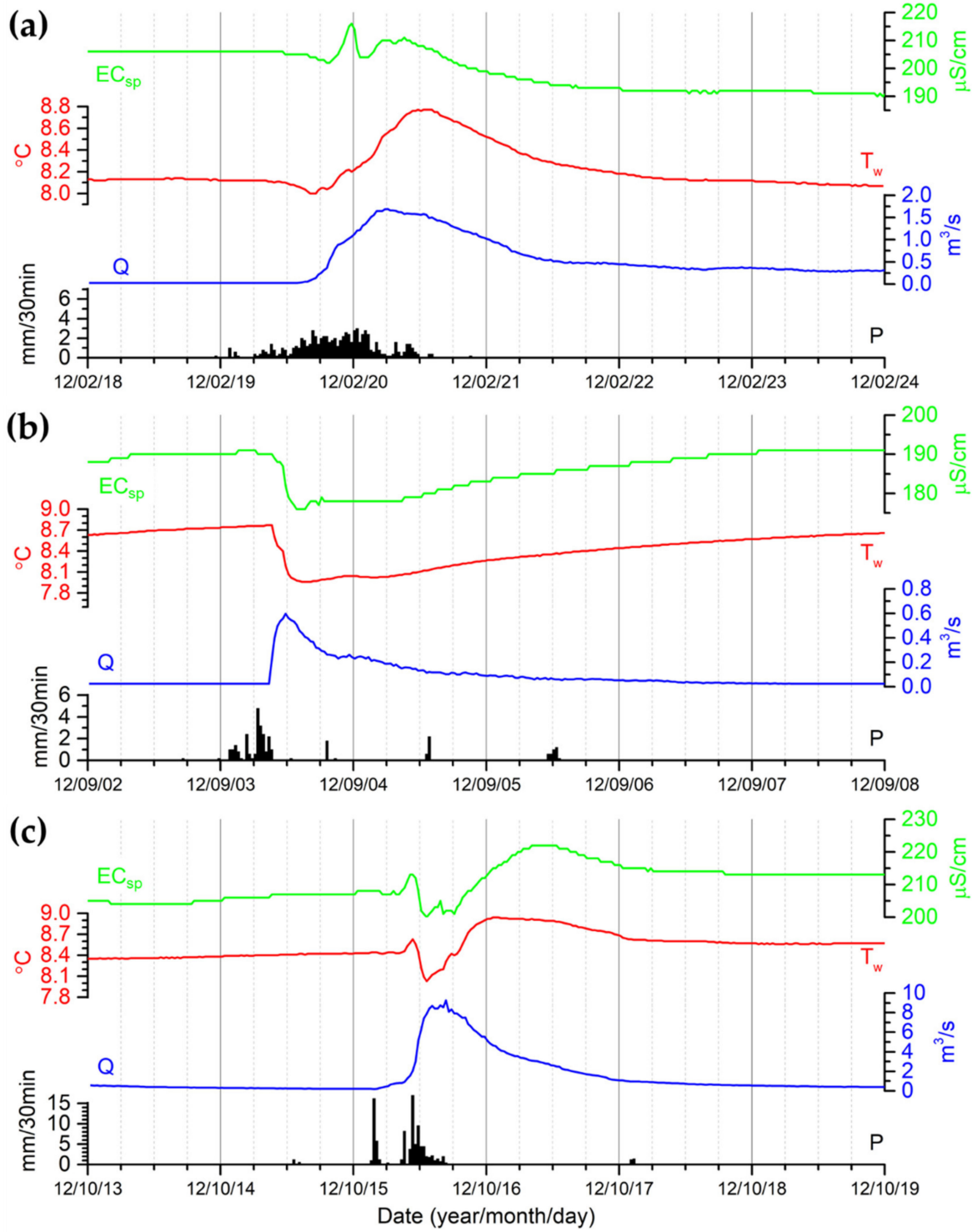

Figure 8. Examples of storm HTC-graphs observed at the Pollaccia spring. Each one highlights some features of the spring hydrodynamic response to precipitation: (**a**) low-magnitude winter storm event (event n. 6, see also Figure 4, Table 4 and SM); (**b**) small-scale discharge peak at the end of the summer drought (n. 18); (**c**) high-magnitude autumnal storm event (n. 23).

The second HTC-graph (Figure 8b) shows a weak discharge peak (Q_c = 0.6 m^3/s) that occurred at the end of the summer drought phase. The rainfall event that triggered the discharge increase was more concentrated than in the previous example, and it showed a P_{rate} of 3 mm/h for a precipitation interval of 7.5 h. The thermograph and chemograph

showed in-phase oscillations, and both T_w and EC_{sp} had marked decreases during the peak flow (−0.8 °C and −14 µS/cm). The lag times between T_P/EC_P and Q_c were short and positive (2–3 h); therefore, T_w and EC_{sp} oscillations occurred after Q_c. All of the parameters recovered to pre-storm values after 2–3 days.

The third HTC-graph shows a strong recharge event that happened during autumn when the flow rate reached 9.3 m^3/s (Figure 8c), and the discharge responded very quickly to the onset of precipitation (Δt_S = 1 h). Water temperature and electrical conductivity showed, again, very similar trends: both experienced small increases that were followed by two consecutive negative and positive peaks. These oscillations had an amplitude of 0.6 °C for T_w and 13 µS/cm for EC_{sp}. The chemograph and thermograph sequences can be explained as follow: first, a small-scale piston flow occurred, followed by a dilution effect possibly caused by a proximal contribution of sinking runoff water. Finally, a sustained piston flow effect was observed during the hydrograph's falling limb. It appears that the thermograph mirrors the chemograph's trends (opposing phase) during recharge events that were influenced by snow melting; in fact, this behavior was observed mostly in April 2013; otherwise, they showed in-phase oscillations.

Overall, dilution effects were observed during most of the monitored storm events, regardless of the flow conditions, whereas piston flow phenomena were more common during the low-flow winter phase (Table 4). In cases of a combination of dilution and piston effects, the latter one was either related to moderate (up to 10 µS/cm) EC_{sp} increases at the beginning of the rising limb or to small but long-lasting EC_{sp} rises during the recession phase.

5. Discussion

5.1. Spring Recharge/Discharge Hydrodynamics

The monitoring of this karst system shows a complex hydrodynamic behavior that depends firstly on its architecture (i.e., recharge type and storage) and climate conditions (i.e., wet/dry phases and lag seasonality) and, secondarily, on meteorological factors. The response to storm events was rather fast, within a few hours, but it shows a complex pattern probably due to the different recharge times in the various sectors. The Pollaccia catchment is characterized by a relevant runoff contribution (allogenic recharge) and concentrated recharge through several sinking streams (Figure 2c). Usually, temperature and conductivity decrease during the major flood phase (Figure 8b). This suggests a typical "dominant drain" pattern [10], with mainly free-surface flow in well-karstified conduits, where the neo-infiltrating water quickly replaces the water circulating in the system (prevalent substitution/dilution). This appears in contrast to the direct knowledge of the outlet morphology obtained by diving exploration, showing a valclusian-type submerged conduit explored for over 500 m in length and approximately 120 m in depth. Therefore, the deep phreatic conduits, which are responsible for the piston flow phenomena at the beginning of the rising limb, are probably limited to the submerged section close to the outflow (Figure 8). However, the drainage system is composed of sectors with different hydrodynamic behaviors. Surely, there is a rapid drainage system, also fed by sinking streams, that is responsible for most of the observed dilution phenomena (e.g., Figure 8b) and of the overall short P-Q lags. Similar lags were found only for karst springs that drain smaller catchments, otherwise the lags were longer [17,18,44,45]. However, other Apuan karst springs showed similar lags; therefore, the local setting plays a fundamental role in the functioning of these karst systems [46].

The spring always has a rapid response to precipitation, sometimes due to the arrival of runoff water that infiltrates along the bed of the Turrite Secca stream and its tributaries in the spring proximity. Proximal runoff contribution can be highlighted by small decreases of T and EC that sometimes occur at the very beginning of the storm hydrograph's rising limb (e.g., Figure 8a) or by opposite EC-T peaks during strong floods events (e.g., the 2012 AR events; Figure 4). Sometimes, the rapid response to infiltration was marked also by small piston effects during the rising limb of the storm HTC-graphs (Figure 8a,c). These phenomena were probably related to the flushing of water that was stored in the proximal

phreatic sector. Then, this water was replaced by neo-infiltrating water that decreased EC to values that were lower than the pre-storm ones (e.g., the falling limb in Figure 8a). Eventually, long-lasting piston flow phenomena were observed during the recession phase of storm HTCs that happened during AR and late SDr (e.g., Figure 8c). These EC increases could reflect the discharge of water from a peripheral phreatic network characterized by a delayed response. The system's complexity and the precipitation pattern also influence the seasonality of the P-Q lags: low-flow conditions occurred in both winter and summer, but the hydrodynamic response was faster during the latter phase than in the former one. Probably, runoff is more efficient during summer (when the groundwater contribution from the whole catchment is limited). Moreover, summer storms were more intense than winter storms as demonstrated by the P_{rate} (mean/median values of 6.61/5.20 mm/h for the former and 2.52/2.61 mm/h for the latter; SM). The $\Delta t\ lag_{(P-Qc)}$ were shorter during the spring discharge events than during the autumn recharge events, despite the formers having lower P_{tot} (mean/median = 55.35/47.20) and P_{rate} (mean/median = 6.66/4.50 mm/h) than the latter ones (P_{tot} mean/median = 106.82/67.2 mm and P_{rate} mean/median = 7.31/6.67 mm/h; SM). The EC/T-Q lags also reflect the complexity of this aquifer: EC_{sp} and T_w usually show in-phase oscillations, but their peaks were slightly shifted with the EC_{sp} peaks that occurred after the T_w ones.

Aquifers can modulate differently the variation of the hydraulic head, heat transfer, and mineralization for a single infiltration event, resulting in asynchronous responses of each parameter. These differential signal lags are usually related to the aquifer's intrinsic properties and, secondarily, to the characteristics of the recharge event [17]. Therefore, the asynchronicity could be explained by differential contributions from distinct sub-systems with nonreactive transport occurring in master conduits and with low matrix storage in the saturated zone, partly like the "tributary mixing" effects described in [20].

5.2. Drought HTC-Graph Analysis

A particular phenomenon of EC_{sp} variation, apparently not linked to infiltrative events, was observed during the anomalous, prolonged winter drought with low-flow rates (Figure 9a). Since 2012/01/05, the EC_{sp} underwent a regular increase from 179 up to 228 µS/cm; then, it decreased slowly and regularly until new and intense precipitations occurred a month later. This trend could be the effect of the superimposition of the exhaustion curves of two (or more) distinct feeding sub-systems characterized by waters with different conductivities. The main sub-system (ss_{main}, Figure 9) collects water from the western, southern, and northern sectors of the catchment (M. Fiocca, M. Sumbra, M. dei Ronchi, M. Corchia northern side, and M. Freddone; Figures 2 and 9b). The structural setting here consists of tight isoclinal folds with steeply dipping layers that allow for both infiltration (usually focused through sinkholes) and runoff over the marble outcrops, whereas runoff alone occurs over the noncarbonate terrains that cover approximately 50% of the sub-catchment surface. This structural arrangement has limited the formation of a well-developed epikarst that could regulate/delay the transfer of infiltrating water (Figure 1a). The ss_{main} recharge area is wide, it is characterized by a lower hydraulic gradient and the water mostly flows in epiphreatic conditions as suggested by some tracer tests [41,47]. A peripheral separated feeding sub-system occurs in the southeastern sector of the catchment on the Panie Group northern ridge (ss_{panie}; Figure 9). This sub-system is characterized by a highly developed epikarst (see Figure 1b) that probably has a relevant role in regulating the transmission of recharge water to the phreatic zone.

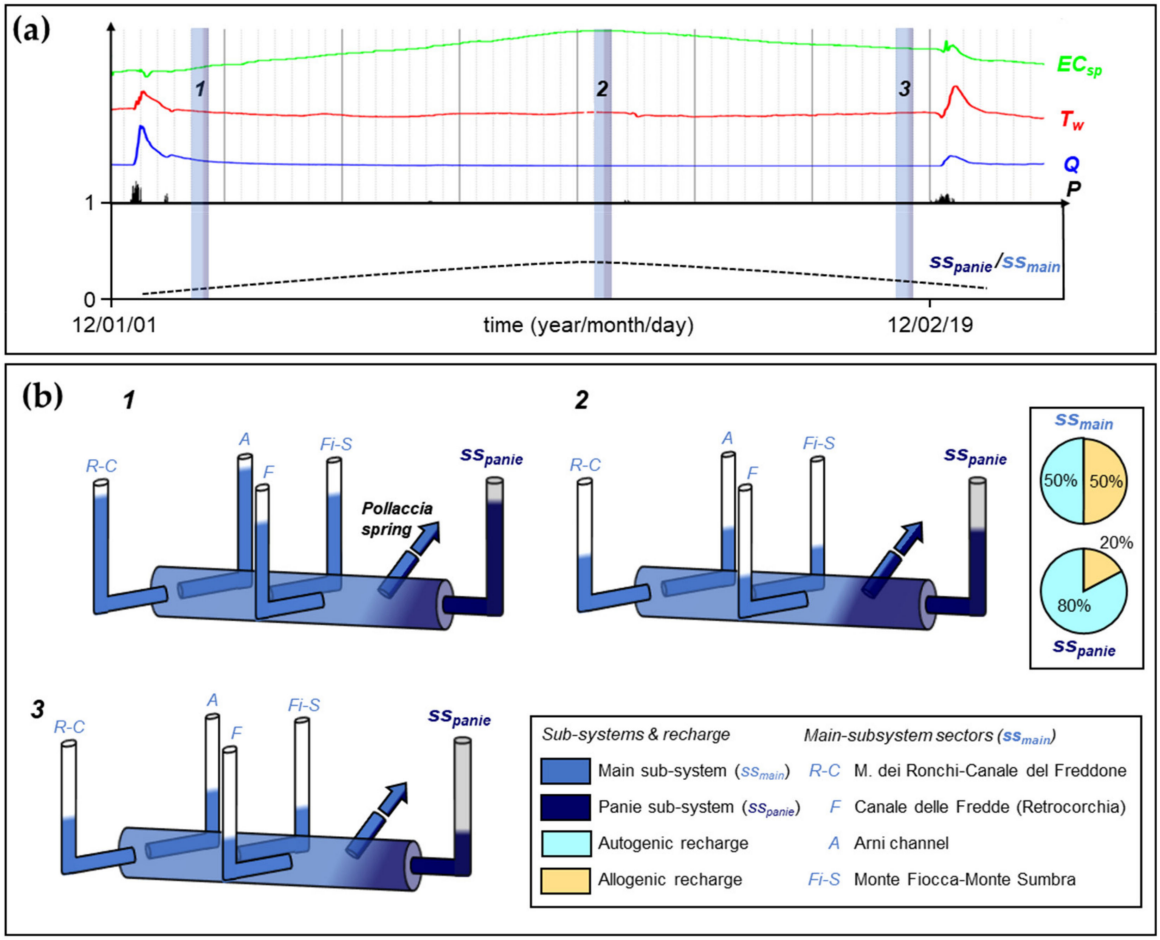

Figure 9. (**a**) Water discharge Q, T_w, and EC_{sp} graphs and a ratio expressing the relative contribution to spring discharge of the two sub-systems from 1 January 2012 to 26 February 2012, showing a period with no significant precipitation events; (**b**) groundwater flow models during steps 1, 2, and 3 depending on the proportions of allogenic/autogenic recharge for the two subsystems.

The ss_{main} has a hydrodynamic behavior more impulsive than the ss_{panie} that is characterized by extensive marble outcrops with sub-horizontal bedding and pervasive fracturing. These conditions led to (a) the development of an epikarst capable of retaining water; (b) diffuse, fast recharge by percolation through vertical fracture networks; (c) probably the absence of fast vadose flow through sub-horizontal master conduits. The association of the pervasive, vertical fractures and the horizontal bedding led to the development of a karst system with no preferential underground drainage path. Water quickly percolates in a diffuse way through the vertical fractures, but a part of it is retained in the narrowest fissures and along the bedding surfaces, leading to a significant epikarst water storage. Consequently, precipitation causes a dual response of this sub-system: a rapid hydraulic gradient increase due to the fact of rapid feeding through the widest fractures and a slow release of water from the diffuse epikarst. This latter contribution to discharge was volumetrically smaller than the former one, but it can be recognized during drought phases. The water table fluctuates more in the ss_{main} sub-system than in the ss_{panie}, although the former one contributes to approximately three-quarters of the Pollaccia baseflow. As a result, the ss_{panie} contribution to discharge became more relevant during the first part the low-flow winter phase (increasing the ratio ss_{panie}/ss_{main}; Figure 9a) once the impulsive response of the ss_{main} had ended (from "1" to "2" in Figure 9) and the epikarst's more mineralized water were progressively released. However, the ratio ss_{panie}/ss_{main} started to decrease again after a month due to the exhaustion of the ss_{panie} epikarst's contribution (from "2" to "3" in Figure 9).

6. Conclusions

The behavior of the Pollaccia spring appears to be influenced by three different types of recharge, groundwater flow, and storage: (1) allogenic runoff recharge in the noncarbonate sectors; (2) autogenic concentrated recharge over the steeply dipping marble outcrops, characterized by fast epiphreatic flow through master conduits and reduced epikarst storage; (3) autogenic recharge through highly fractured, gently dipping marble outcrops, characterized by quick hydraulic pressure transfer to the phreatic zone and relevant epikarst storage. The complexity of the spring feeding system coupled with the local climate conditions determine specific hydrodynamic responses for each hydrological phase. The main sub-system storage contributes to most of the Pollaccia discharge, but its structure (i.e., recharge mode and storage) determines an impulsive response to infiltration. Therefore, the ss_{main} sustains the Pollaccia baseflow, but its water level fluctuates more impulsively than the ss_{panie} one. The latter sub-system has a lower storage capacity than the former one, but its epikarst storage can contribute significantly to baseflow, although not for long time intervals. It is important to stress that each sector's contribution to the spring discharge can be recognized by analyzing both the spring hydrodynamic response to infiltration events (i.e., the storm HTC-graphs) and the low-flow phases with no precipitation (i.e., the drought HTC-graphs). In other words, drought phases can allow for the recognition of the contribution of different storage domains in complex hydrogeologic systems. An example of the usefulness of the latter analysis is the anomalous winter drought phase (i.e., its precipitation amount resembled a summer drought phase) observed at the beginning of 2012. The anomalous hydrological conditions permitted to recognize the role of the epikarst storage in the different subsystems to the Pollaccia spring discharge, normally hidden during storms because the flood flow is mostly sustained by the main sub-system. The recognition of different storage components by means of the drought HTC-graph analysis is not a common approach; however, it is promising for karst springs in alpine-like landscapes, such as Pollaccia, because anomalous drought conditions are now becoming progressively more recurrent due to climate change. These findings could be integrated in future research with quantitative dye tracer tests and groundwater dating to develop more precise models.

Supplementary Materials: The following supporting information can be downloaded at: https://www.mdpi.com/article/10.3390/hydrology9050083/s1, Table S1: Storm hydrograph and lag analyses.

Author Contributions: Conceptualization, L.P. and A.N.; methodology, L.P. and A.N.; software, A.N.; validation, L.P. and A.N.; formal analysis, A.N.; investigation, L.P. and A.N.; resources, L.P.; data curation, L.P. and A.N.; writing—original draft preparation, L.P. and A.N.; writing—review and editing, L.P. and A.N.; visualization, A.N.; supervision, L.P.; project administration, L.P.; funding acquisition, L.P. All authors have read and agreed to the published version of the manuscript.

Funding: This research was funded by the Università degli Studi di Firenze (University of Florence) (grant number: PI19ARPAT_APUANO-ARPAT) and by the Federazione Speleologica Toscana.

Data Availability Statement: Precipitation data are available at the website of the Regional Hydrological Service of Tuscany (https://www.sir.toscana.it/consistenza-rete, accessed 1 December 2020). The hydrological data are not readily available, because they will be used for other publications. Requests to access the dataset should be directed to the corresponding author.

Acknowledgments: The authors are indebted to the Federazione Speleologica Toscana (Tuscan Speleological Federation), which provided the devices used for monitoring of the spring.

Conflicts of Interest: The authors declare no conflict of interest. The funders had no role in the design of the study; in the collection, analyses, or interpretation of data; in the writing of the manuscript, or in the decision to publish the results.

References

1. Ford, D.; Williams, P.D. *Karst Hydrogeology and Geomorphology*; John Wiley & Sons: Chichester, UK, 2007.
2. Jukić, D.; Denić-Jukić, V. Groundwater balance estimation in karst by using a conceptual rainfall–runoff model. *J. Hydrol.* **2009**, *373*, 302–315. [CrossRef]
3. Hartmann, A.; Goldscheider, N.; Wagener, T.; Lange, J.; Weiler, M. Karst water resources in a changing world: Review of hydrological modeling approaches. *Rev. Geophys.* **2014**, *52*, 218–242. [CrossRef]
4. Bakalowicz, M. The epikarst, the skin of karst. In *Epikarst, Special Publication*, 9th ed.; Jones, W.K., Culver, D.C., Herman, J., Eds.; Karst Waters Institute: Leesburg, VA, USA, 2004; pp. 16–22.
5. Williams, P.W. The role of the epikarst in karst and cave hydrogeology: A review. *Int. J. Speleol.* **2008**, *37*, 1–10. [CrossRef]
6. Hartmann, A.; Baker, A. Modelling karst vadose zone hydrology and its relevance for paleoclimate reconstruction. *Earth Sci. Rev.* **2017**, *172*, 178–192. [CrossRef]
7. Mangin, A. Karst Hydrogeology. In *Groundwater Ecology*; Gibert, J., Danielopol, D.L., Stanford, J.A., Eds.; Academic Press: New York, NY, USA, 1994; pp. 43–67.
8. White, W.B. Karst hydrology: Recent developments and open questions. *Engin. Geol.* **2002**, *65*, 85–105. [CrossRef]
9. Berglund, J.L. Karst Aquifer Recharge and Conduit Flow Dynamics from High-Resolution Monitoring and Transport Modeling in Central Pennsylvania Springs. Ph.D. Thesis, Temple University, Philadelphia, PA, USA, May 2019.
10. Vigna, B.; Banzato, C. The hydrogeology of high-mountain carbonate areas: An example of some Alpine systems in southern Piedmont (Italy). *Environ. Earth Sci.* **2015**, *74*, 267–280. [CrossRef]
11. Bonacci, O. Karst spring hydrographs as indicators of karst aquifers. *Hydrol. Sci. J.* **1993**, *38*, 51–62. [CrossRef]
12. Goldscheider, N.; Drew, D. *Methods in Karst Hydrogeology*; IAH: International Contributions to Hydrogeology, 26; Taylor & Francis/Balkema: Leiden, The Netherlands, 2014.
13. Desmarais, K.; Rojstaczer, S. Inferring source waters from measurements of carbonate spring response to storms. *J. Hydrol.* **2002**, *260*, 118–134. [CrossRef]
14. Winston, W.E.; Criss, R.E. Dynamic hydrologic and geochemical response in a perennial karst spring. *Water Resour. Res.* **2004**, *40*, 05106. [CrossRef]
15. Nannoni, A.; Vigna, B.; Fiorucci, A.; Antonellini, M.; De Waele, J. Effects of an extreme flood event on an alpine karst system. *J. Hydrol.* **2020**, *590*, 125493. [CrossRef]
16. Liñán Baena, C.; Andreo, B.; Mudry, J.; Carrasco Cantos, F. Groundwater temperature and electrical conductivity as tools to characterize flow patterns in carbonate aquifers: The Sierra de las Nieves karst aquifer, southern Spain. *Hydrogeol. J.* **2009**, *17*, 843–853. [CrossRef]
17. Sánchez, D.; Martín-Rodríguez, J.F.; Mudarra, M.; Andreo, B.; López-Rodríguez, M.; Navas, M.R. Time Lag Analysis of Natural Responses During Unitary Recharge Events to Assess the Functioning of Carbonate Aquifers in Sierra de Grazalema Natural Park (Southern Spain). In *EuroKarst 2016, Neuchâtel. Advances in Karst Science*; Renard, P., Bertrand, C., Eds.; Springer International Publishing: Cham, Switzerland, 2017; pp. 157–167. [CrossRef]
18. Birk, S.; Liedl, R.; Sauter, M. Identification of localised recharge and conduit flow by combined analysis of hydraulic and physico-chemical spring responses (Urenbrunnen, SW-Germany). *J. Hydrol.* **2004**, *286*, 179–193. [CrossRef]
19. Genthon, P.; Bataille, A.; Fromant, A.; D'Hulst, D.; Bourges, F. Temperature as a marker for karstic waters hydrodynamics. Inferences from 1 year recording at La Peyrére cave (Ariège, France). *J. Hydrol.* **2005**, *311*, 157–171. [CrossRef]
20. Perrin, J.; Jeannin, P.Y.; Cornaton, F. The role of tributary mixing in chemical variations at a karst spring, Milandre, Switzerland. *J. Hydrol.* **2007**, *332*, 158–173. [CrossRef]
21. Calligaris, C.; Galli, M.; Gemiti, F.; Piselli, S.; Tentor, M.; Zini, L.; Cucchi, F. Electrical conductivity as a tool to evaluate the various recharges of a Karst aquifer. *Rend. Online Della Soc. Geol. Ital.* **2019**, *47*, 13–17. [CrossRef]
22. Chen, Z.; Hartmann, A.; Wagener, T.; Goldscheider, N. Dynamics of water fluxes and storages in an Alpine karst catchment under current and potential future climate conditions. *Hydrol. Earth Sys. Sci.* **2018**, *22*, 3807–3823. [CrossRef]
23. Nerantzaki, S.D.; Nikolaidis, N.P. The response of three Mediterranean karst springs to drought and the impact of climate change. *J. Hydrol.* **2020**, *591*, 125296. [CrossRef]
24. Fiorillo, F. Spring hydrographs as indicators of droughts in a karst environment. *J. Hydrol.* **2009**, *373*, 290–301. [CrossRef]
25. Fiorillo, F.; Guadagno, F.M. Karst spring discharges analysis in relation to drought periods, using the SPI. *Water Res. Managem.* **2010**, *24*, 1867–1884. [CrossRef]
26. Fiorillo, F.; Revellino, P.; Ventafridda, G. Karst aquifer draining during dry periods. *J. Cave Karst Stud.* **2012**, *74*, 148–156. [CrossRef]
27. Petalas, C.P.; Moutsopoulos, K.N. Hydrogeologic behavior of a complex and mature karst aquifer system under drought condition. *Environ. Processes* **2019**, *6*, 643–671. [CrossRef]
28. Lauritzen, S.E. Karst resources and their conservation in Norway. *Nor. Geogr. Tidsskr. Nor. J. Geogr.* **1991**, *45*, 119–142. [CrossRef]
29. Lauritzen, S.E. Marble stripe karst of the scandinavian caledonides: An endmember in the contact karst spectrum. *Acta Carsologica* **2001**, *30*, 47–79.
30. Filipponi, M.; Jeannin, P.Y.; Tacher, L. Evidence of inception horizons in karst conduit networks. *Geomorphology* **2009**, *106*, 86–99. [CrossRef]

31. Andreo, B.; Carrasco, F.; De Galdeano, C.S. Types of carbonate aquifers according to the fracturation and the karstification in a southern Spanish area. *Environ. Geol.* **1997**, *30*, 163–173. [CrossRef]
32. Despain, J.D.; Stock, G.M. Geomorphic history of Crystal Cave, Southern Sierra Nevada, California. *J. Cave Karst Stud.* **2005**, *67*, 92–102.
33. Antonellini, M.; Nannoni, A.; Vigna, B.; De Waele, J. Structural control on karst water circulation and speleogenesis in a lithological contact zone: The Bossea cave system (Western Alps, Italy). *Geomorphology* **2019**, *345*, 106832. [CrossRef]
34. Doveri, M.; Piccini, L.; Menichini, M. Hydrodynamic and geochemical features of metamorphic carbonate aquifers and implications for water management: The Apuan Alps (NW Tuscany-Italy) case study. In *Karst Water Environment*; Younos, T., Schreiber, M., Kosič Ficco, K., Eds.; Springer International Publishing: Cham, Switzerland, 2019; pp. 209–249.
35. Piccini, L. Evolution of karst in the Alpi Apuane (Italy): Relationships with the morphotectonic history. *Suppl. Geogr. Fis. E Din. Quat. III* **1998**, *4*, 21–31.
36. Kligfield, R.; Hunziker, J.; Dallmeyer, R.D.; Schamel, S. Dating of deformational phases using K-Ar and $^{40}Ar/^{39}Ar$ techniques: Results from the Northern Apennines. *J. Struct. Geol.* **1986**, *8*, 781–798. [CrossRef]
37. Carmignani, L.; Kligfield, R. Crustal extension in the Northern Apennines: The transition from compression to ex-tension in the Alpi Apuane Core Complex. *Tectonics* **1990**, *9*, 1275–1303. [CrossRef]
38. Conti, P.; Di Pisa, A.; Gattiglio, M.; Meccheri, M. Prealpine basement in the Alpi Apuane (Northern Apennines, Italy). In *Pre-Mesozoic Geology in the Alps*; Von Raumer, J.F., Neubauer, F., Eds.; Springer Verlag: Berlin/Heidelberg, Germany, 1993; pp. 609–621.
39. Ottria, G.; Molli, G. Superimposed brittle structures in the late-orogenic extension of the Northern Apennine: Results from the Carrara area (Alpi Apuane, NW Tuscany). *Terra Nova* **2000**, *12*, 52–59. [CrossRef]
40. Piccini, L. Acquiferi carbonatici e sorgenti carsiche delle Alpi Apuane. In Proceedings of the Le Risorse Idriche Sotterranee Delle Alpi Apuane: Conoscenze Attuali e Prospettive di Utilizzo, Forno di Massa, Italy, 22 June 2002; pp. 41–76.
41. Piccini, L.; Giannini, E.; Malcapi, V.; Poggetti, E.; Steinberg, B. Monitoraggio idrodinamico di un sistema carsico: Risultati preliminari di un anno d'indagini alla sorgente Pollaccia (Alpi Apuane—Toscana). In Proceedings of the La Ricerca Carsologica in Italia, Fabrosa Soprana, Italy, 22–23 June 2013; pp. 147–154.
42. USDA. NRCS. Chapter 3. Hydraulics. In *National Engineering Handbook, Part 650, Engineering Field Handbook*; USDA: Washington, DC, USA, 2001.
43. Kresic, N.; Stevanovic, Z. *Groundwater Hydrology of Springs: Engineering, Theory, Management and Sustainability*; Butterworth-heinemann: Oxford, UK, 2009.
44. Cholet, C.; Steinmann, M.; Charlier, J.B.; Denimal, S. Comparative study of the physicochemical response of two karst systems during contrasting flood events in the French Jura Mountains. In *Hydrogeological and Environmental Investigations in Karst Systems. Environmental Earth Sciences*; Andreo, B., Carrasco, F., Durán, J., Jiménez, P., LaMoreaux, J., Eds.; Springer: Berlin/Heidelberg, Germany, 2015; Volume 1, pp. 1–9. [CrossRef]
45. Adji, T.N.; Bahtiar, I.Y. Rainfall–discharge relationship and karst flow components analysis for karst aquifer characterization in Petoyan Spring, Java, Indonesia. *Environ. Earth Sci.* **2016**, *75*, 1–10. [CrossRef]
46. Piccini, L.; Nannoni, A.; Poggetti, E. Hydrodynamic of karst aquifers in metamorphic carbonate rocks: Results from spring monitoring in the Apuan Alps (Tuscany, Italy). *Hydrogeol. J.* **2022**. *under review*.
47. Piccini, L. Sui risultati della prova di colorazione all'abisso F. Orsoni—Vetricia (Apuane). *Talp* **1989**, *1*, 48–50.